John J. Degnan and John J. Zayhowski, Proc 11th International Workshop on Laser Ranging, Deggendorf, Germany, Sept. 21-25, 1998, pp. 453-468

SLR2000 MICROLASER PERFORMANCE: THEORY vs EXPERIMENT

John J. Degnan
Geoscience Technology Office
NASA Goddard Space Flight Center
Greenbelt, MD 20771-0003 USA

and

John J. Zayhowski
MIT Lincoln Laboratory
244 Wood St.
Lexington, MA 02420-9108 USA

ABSTRACT

An improved model for passively Q-switched lasers has been developed which explicitly includes the effects of level lifetimes and excited state absorption in the saturable absorber as well as unequal beam diameters in the gain and absorbing media. The optimization equation yields the value of the parameter $\rho = \ln(n_i/n_f)$, where n_i and n_f are the inversion population densities before and after Q-switching, which maximizes the single-pulse energy. Using this result, the optimum absorber transmission, mirror reflectivity, and pulse energy (and the corresponding peak power and pulse width) can be computed sequentially via simple formulas. As in an earlier theory which did not include excited state absorption, the optimized parameters can be expressed as functions of two variables, α_{eff} and z_{eff}, which are slight modifications of the variables α and z previously introduced by one of the authors for passively Q-switched lasers having no excited state absorption and equal beam areas in the gain and absorbing media. In the new model, we define $\alpha_{eff} = E_{sat}^{amp}/E_{sat}^{abs} = \alpha A/A_s$, equal to the ratio of the laser saturation energy to the absorber saturation energy, and $\beta = 1/z_{eff} = 1/\mathrm{FOM} + (1-1/\mathrm{FOM})/z$. In these parameter definitions, A and A_s are the beam areas in the gain and absorber media respectively, $z = 2\ln G_0/L$ as before, G_0 is the single-pass small-signal gain, L is the round-trip dissipative loss, and $\mathrm{FOM} = \sigma_{gs}/\sigma_{es}$ is the absorber figure of merit corresponding to the ratio of the ground state to excited state cross-sections.

The performance predictions of this new model are compared to prototype SLR2000 transmitters developed under a joint program between the NASA Goddard Space Flight Center and MIT Lincoln Laboratory. The goal of this joint program is to investigate the feasibility of an advanced, higher-power, microlaser oscillator which would meet the SLR2000 energy and pulse width goals of 130 μJ and 150 psec at 532 nm without the need for a passive multipass amplifier (which is assumed in our baseline SLR2000 transmitter design). The first phase of this program, begun in October 1997, has investigated quasi-CW pumped Nd:YAG microlasers which have successfully operated at repetition rates between 500 and 2000 Hz. Several different devices, between 6 and 24 mm in length, were constructed. All were end-pumped by a single fiber-coupled AlGaAs diode laser array emitting 3 to 16 W at the Nd:YAG pump wavelength of 808 nm. As expected, there is a tradeoff between pulse width and pulse energy. At 500 Hz in quasi-CW pumped mode, one microlaser, with a physical length of 7.25 mm, produced 200 μJ in a 300 psec pulse width while a second microlaser, with a physical length of 10.5 mm, produced 250 μJ in a 380 psec pulse width. The spatial mode was nominally TEM_{00} under the reported operating conditions. Frequency doubling should produce the specified energy and reduce the pulse width slightly at 532 nm, but the pulse width, at present, is still somewhat longer than desired. Efforts are continuing to further optimize the design. Furthermore, the current pump powers are near the maximum ratings for the single array and it may be necessary to use more diodes in a derated mode in order to achieve long life and reliability.

John J. Degnan and John J. Zayhowski, Proc 11th International Workshop on Laser Ranging, Deggendorf, Germany, Sept. 21-25, 1998, pp. 453-468

1. INTRODUCTION

NASA's fully automated SLR2000 Satellite Laser Ranging system is designed to be inherently eyesafe anywhere within the external beam. In order to achieve this goal, the energy flux at the exit pupil of the telescope is kept below a value $F_{max} = 0.5\ \mu J/cm^2 / [f_{QS}\ \tau]^{1/4}$ as dictated by ANSI safety standards for Q-switched laser pulses where f_{QS} = 2000/sec is the Q-switching rate and $\tau = 0.25$ sec is the standard integration time for visible light.

Even if the transmitted beam fills the 40-cm aperture telescope, the single-pulse energy out of the telescope aperture is limited to about 130 μJ at a wavelength of 532 nm. Assuming a nominal doubling efficiency on the order of 50 to 60%, a 2 KHz laser fire rate, and an estimated throughput efficiency of 60% for the SLR2000 transmitter optics, one might need to generate between 360 and 440 μJ per pulse or between 720 and 880 mW of average power at the fundamental Nd:YAG wavelength of 1064 nm.

As of the last workshop in Shanghai, demonstrated microlaser energies and powers were typically more than an order of magnitude smaller than the SLR2000 requirements. Therefore, a design based on a microlaser oscillator followed by a passive multipass amplifier, both of which were pumped by CW diode laser arrays operating at 808 nm, was proposed [1]. On the other hand, our initial optimization modeling [1,2] suggested that a much simpler oscillator-only configuration, meeting the full range of SLR2000 specifications, was feasible. As a result, the Goddard Space Flight Center entered into an exploratory Joint Program with MIT Lincoln Laboratory to develop a series of higher power Nd:YAG microlaser oscillators.

In parallel with the experimental effort at MIT Lincoln Laboratory, various improvements to the passively Q-switched laser optimization model were made at GSFC and elsewhere [3,4,5]. The most important of these improvements was the inclusion of excited state absorption which is an important process in the Cr^{4+}:YAG passive Q-switch and had not been accounted for in earlier GSFC theories [1,2]. Although not particularly relevant to the ultrashort pulse microlasers needed for SLR2000, the improved theory presented here has also been modified to accommodate unequal beam areas in the gain and absorbing media.

2. GENERAL PASSIVE Q-SWITCH EQUATIONS

The output pulse energy of a general Q-switched laser (active or passive) is given by the equation [2,6]

$$E = \frac{h\nu A}{2\gamma\sigma}\,\rho \ln\left(\frac{1}{R}\right), \tag{1}$$

where $h\nu$ is the laser photon energy, A is the effective beam area in the laser medium, σ is the spectroscopic cross-section of the laser transition, γ is the inversion reduction factor [6], R is the output mirror reflectivity, and the parameter ρ is defined by the equation [2,6]

$$\rho = \ln\left(\frac{n_i}{n_f}\right), \tag{2}$$

where n_i is the population inversion density at the onset of Q-switching and n_f is the final population inversion density following the passage of the Q-switched pulse. For a general passively Q-switched laser, the parameter ρ in Eq. (1) is given by the solution to the transcendental equation

$$\frac{1-\frac{1}{\rho}\left(1-e^{-\rho}\right)}{1-\frac{1}{\alpha\rho}\left(1-e^{-\alpha\rho}\right)} = \varphi \tag{3a}$$

where

$$\varphi \equiv (1-\delta)\frac{\ln\left(\frac{1}{T_0}\right)}{\ln G_0}. \qquad . \tag{3b}$$

In Eq. (3), T_0 is the unsaturated one-way transmission of the saturable absorber, α is the ratio of the laser saturation energy to the absorber saturation energy defined by

$$\alpha \equiv \frac{E_{sat}^{gain}}{E_{sat}^{abs}} = \frac{\sigma_{gs}}{\gamma\sigma}\frac{A}{A_s} \tag{4}$$

where A and A_s are the effective beam areas in the gain and saturable absorber media respectively,

$$\delta \equiv \frac{1}{FOM} \equiv \frac{\sigma_{es}}{\sigma_{gs}} \tag{5}$$

is the inverse of the absorber "Figure of Merit" [7], and σ_{gs} and σ_{es} are the absorption cross-sections of the ground and excited states, respectively. In the microlasers considered here, $A = A_s$.

The peak power of the general passively Q-switched laser can be computed via the equation

$$P = \frac{h\nu A \ln G_0}{\gamma\sigma\tau_r}\ln\left(\frac{1}{R}\right)\left[\left(1-\frac{1}{\alpha}\right)(1-x_f)+(1-\varphi)\ln x_f\right] \quad , \tag{6a}$$

where x_f is the solution to

$$1 - x_f - \varphi\left(1-x_f^{\alpha}\right) = 0 . \tag{6b}$$

An approximate expression for the laser pulse width is then obtained by dividing (6a) into (1), yielding

$$\tau_p \cong \frac{E}{P} = \frac{\tau_r}{2\ln G_0}\frac{\rho}{\left[\left(1-\frac{1}{\alpha}\right)(1-x_f)+(1-\varphi)\ln x_f\right]}. \tag{7}$$

3. OPTIMIZED LASER EQUATIONS

Using a Lagrange multiplier technique as outlined in [2], one can generate an optimization equation whose root is the value of ρ which maximizes the laser output energy for the given set of initial conditions. Using the results of References 2 through 5, the optimization equation can be shown to be a function of two variables, α and β, and is given by

$$\frac{1-e^{-\rho}}{1-\frac{1}{\alpha\rho}\left(1-e^{-\alpha\rho}\right)}+\frac{1-\frac{1}{\rho}}{1-\frac{1}{\alpha\rho}\left(1-e^{-\alpha\rho}\right)}\left[1-\frac{1-e^{-\alpha\rho}}{1-\frac{1}{\alpha\rho}\left(1-e^{-\alpha\rho}\right)}\right]=1-\beta \tag{8}$$

where α is given by Eq. (4) ,

$$\beta\equiv\frac{1}{z_{eff}}\equiv\delta+\frac{1}{z}(1-\delta)\equiv\delta+\frac{L}{2\ln G_0}(1-\delta) \quad , \tag{9}$$

and L is the round-trip loss exclusive of the output mirror transmission and saturable absorption losses which are accounted for separately in the optimization theory [2]. From (9), β can take on values within the range $\delta \le \beta \le 1$. Note that, as $\delta \to 0$ (i.e. no excited state absorption), $\beta \to 1/z$ and Eq. (6) reduces to a form equivalent to the optimization equation (21) in [2]. In the active Q-switching limit as $\delta \to 0$ and $\alpha \to \infty$, the optimization equation (6) reduces to the simple solution $\rho = \ln(z)$ in agreement with Eqs. (6b) and (10b) in [6].

Once α and β have been specified, the solution to Eq. (8), ρ_{opt}, can be obtained using a numerical root solver such as the "root" function in Mathcad™. One can then sequentially compute all of the optimized parameters including the optimum absorber transmission,

$$T_{opt}=G_0^{-\frac{\varphi_{opt}}{1-\delta}} \quad \text{where} \quad \varphi_{opt}=\frac{1-\frac{1}{\rho_{opt}}\left(1-e^{-\rho_{opt}}\right)}{1-\frac{1}{\alpha\rho_{opt}}\left(1-e^{-\alpha\rho_{opt}}\right)} \quad , \tag{10}$$

the optimum output mirror reflectivity,

$$R_{opt}=G_0^{-\psi_{opt}} \quad \text{where} \quad \psi_{opt}=2\left[1-\frac{L}{2\ln G_0}-\frac{\varphi_{opt}}{1-\delta}\right] \quad , \tag{11}$$

and the maximum laser output energy ,

$$E_{opt}=\frac{h\nu A\ln(G_0)}{\gamma\sigma}\frac{\rho_{opt}\psi_{opt}}{2}=F_{sat}^{gain}\ln(G_0)A\frac{\rho_{opt}\psi_{opt}}{2}, \tag{12}$$

where F_{sat}^{gain} is the pulse width-dependent saturation flux [9]. The peak power and pulse width of the energy-optimized laser can now be computed by substituting ρ_{opt} and φ_{opt} for ρ and φ , respectively, in Eqs. (6) and (7).

4. MICROLASER CONSTRUCTION

Zayhowski et al [7] have reported experimental results on seven different microlaser devices. Their general construction and physical characteristics are summarized in Figure 1 and Table 1, respectively. The prefixes "MP" and "HP" in Table 1 denote "medium power" and "high power" respectively. The four high power devices were constructed under the GSFC microlaser program at MIT Lincoln Laboratory. The gain medium is Nd^{3+}:YAG and

the saturable absorber is Cr^{4+}:YAG. The high power "HP" devices include undoped YAG end caps at the input and/or output ends of the oscillator as in Figure 1. These are used to increase the surface damage thresholds of the devices. Since there is no absorption of pump or laser radiation in the undoped materials, thermal stress at the YAG/dielectric and dielectric/air coatings is reduced. Furthermore, the polished ends of the individual crystals are optically contacted and diffusion bonded by heating the crystals just below the melting point of YAG which virtually eliminates the potentially damage-prone interfaces between doped and undoped materials. In all cases, the output mirror was coated directly onto the final YAG crystal, as in Figure 1, and the input crystal was coated to give high transmission at the diode pump wavelength of 808 nm and high reflectivity (>99.9%) at the fundamental laser wavelength of 1064 nm.

The crystals were cut to a nominal 2 x 2-mm square cross-section and were bonded at the bottom to a gold-coated oxygen-free copper heat sink with thermally conducting epoxy. For high repetition rate operation of devices pumped by 10 W or more, it was necessary to heat sink the lasers from the top as well as the bottom to give a symmetrical thermal profile. More detail regarding the construction and operation of these lasers can be found elsewhere [7,8].

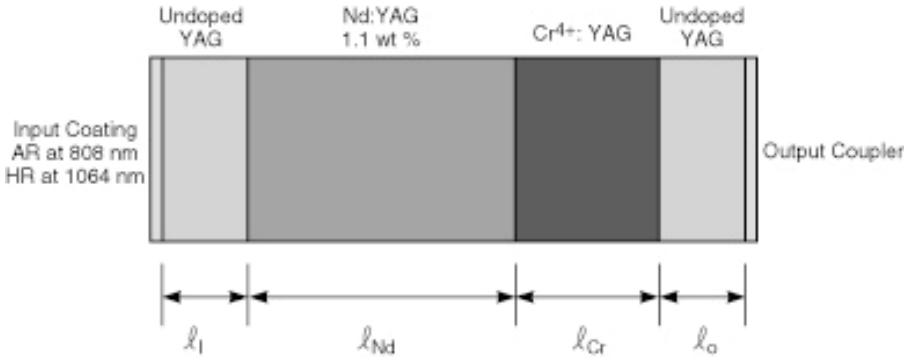

Figure 1: Construction of typical high power microlaser.

Table 1 lists the lengths of the individual segments of the microlaser, the absorption per unit length of the Q-switching saturable absorber (which can be modified via different Cr^{4+} doping concentrations), and the reflectivity of the output mirror. The single-pass transmission of the absorber was computed using the equation $T = \exp(-\alpha_a l_{Cr})$ where α_a and l_{Cr} are given in Table 1.

Device	Input YAG cap l_i (mm)	Nd:YAG l_{Nd} (mm)	Cr^{4+}:YAG l_{Cr} (mm)	Output YAG cap l_o (mm)	Cr^{4+}:YAG Absorption α_a (cm^{-1})	Single-Pass Abs. Trans. T(%)	Output Coupler R (%)
MPMCL-1	**0**	**3**	**3**	**0**	**1.5**	**63.7**	**60**
MPMCL-2	**0**	**3**	**3**	**0**	**1.5**	**63.7**	**60**
MPMCL-3	**0**	**3**	**3**	**12**	**1.5**	**63.7**	**60**
HPMCL-1	**1**	**3**	**1.5**	**1**	**6**	**40.6**	**40**
HPMCL-2	**1**	**4**	**6**	**1**	**1.5**	**40.6**	**40**
HPMCL-3	**1**	**3**	**2.25**	**1**	**6**	**25.9**	**26**
HPMCL-4	**1**	**4**	**2.25**	**3**	**6**	**25.9**	**26**

Table 1: Construction details of various microlasers developed under the joint GSFC/MITLL program.

5. EXPERIMENT VS THEORY

Zayhowski *et al* [7] have reported the results of eleven different experiments conducted with the aforementioned seven devices; these are summarized in Table 2. In all cases, the microlasers were end-pumped at a 500 Hz rate with

rectangular pulses of optical power which were switched off at the first sign of lasing so that pumping did not significantly extend beyond the onset of Q-switching. The optical pump power was delivered from a linear laser diode array via a fiber optic cable. In experiments 1, 2, 3 and 7, the fiber had a 100-μm diameter and a numerical aperture (NA) of 0.2. In the other experiments, the output of a 250-μm-diameter fiber with NA = 0.2 was focused with approximately 0.5 magnification into the laser medium. The experiments included measurements, at the fundamental Nd:YAG wavelength of 1064 nm, of the pulse energy, pulse width, and beam waist radius (center to $1/e^2$ intensity point). These measurements were then used to compute the peak power, peak intensity, and peak fluence values shown in the table. The microlasers operated in a nominal TEM_{00} mode during all of these experiments. Peak intensities up to 10 GW/cm^2 were generated, which allowed high conversion efficiencies in nonlinear crystals at the second, third, and fourth harmonics of Nd:YAG. Figure 2 shows the final packaged microlaser, which can include up to four nonlinear crystals for frequency conversion.

Exp. #	Device	Pump Power (W)	Pulse Energy (μJ)	Pulse Width (psec)	Beam Waist (μm)	Peak Power (KW)	Peak Intensity (GW/cm^2)	Peak Fluence (J/cm^2)
1	**MPMCL-1**	**3**	**30**	**700**	**60**	**37**	**0.65**	**0.53**
2	**MPMCL-2**	**3**	**40**	**1200**	**70**	**29**	**0.37**	**0.52**
3	**MPMCL-3**	**5**	**65**	**2200**	**85**	**25**	**0.22**	**0.57**
4	**MPMCL-1**	**10**	**100**	**650**	**85**	**132**	**1.16**	**0.88**
5	**MPMCL-2**	**10**	**150**	**1000**	**100**	**129**	**0.82**	**0.95**
6	**MPMCL-3**	**10**	**180**	**2000**	**120**	**77**	**0.34**	**0.80**
7	**HPMCL-1**	**3**	**70**	**400**	**55**	**150**	**3.2**	**1.5**
8	**HPMCL-1**	**10**	**130**	**390**	**70**	**286**	**3.7**	**1.7**
9	**HPMCL-2**	**10**	**225**	**700**	**90**	**276**	**2.2**	**1.8**
10	**HPMCL-3**	**11**	**200**	**310**	**60**	**554**	**9.8**	**3.5**
11	**HPMCL-4**	**15**	**250**	**380**	**60**	**565**	**10.0**	**4.4**

Table 2: Device output characteristics determined experimentally at a repetition rate of 500 Hz.

Theoretical computations were made using both the general non-optimized equations and the optimized equations. In comparing the experimental and theoretical results, the following assumptions were made:

(1) The roundtrip dissipative loss, L, was assumed to be negligibly small compared to the roundtrip gain so that $L \cong 0$ and $\beta \cong \delta$. (It is worth noting that in the limit of zero loss, the quantities $\rho(\alpha,\delta)$, $\varphi(\alpha,\delta)$ and $\psi(\alpha,\delta)$ in Eqs. (8) through (12) are fixed for a particular combination of gain medium and saturable absorber materials and the optimum mirror reflectivities and absorber transmissions vary as the small signal gain to a fixed power.)

(2) For the purposes of the output energy and peak power calculations, the beam area was initially assumed to be constant and equal to the effective area of the TEM_{00} mode, i.e. $A_{00} = \pi\omega^2/2$, where ω is the experimentally determined waist value given in Table 2.

(3) The initial gain at the onset of Q-switching was computed based on the threshold condition for lasing, i.e. $G_0^2 T_0^2 R \exp(-L) = 1$.

(4) The saturable absorber cross-sections for the ground and excited states were assumed to be $\sigma_{gs} = 7 \times 10^{-18}$ cm^2 and $\sigma_{es} = 2 \times 10^{-18}$ cm^2 as measured by Burshtein et al [10] .

(5) The spectroscopic cross-section and inversion reduction factor for Nd:YAG were assumed to be $\sigma = 6.5 \times 10^{-19}$ cm^2 [11] and $\gamma = 0.41$ [9] respectively.

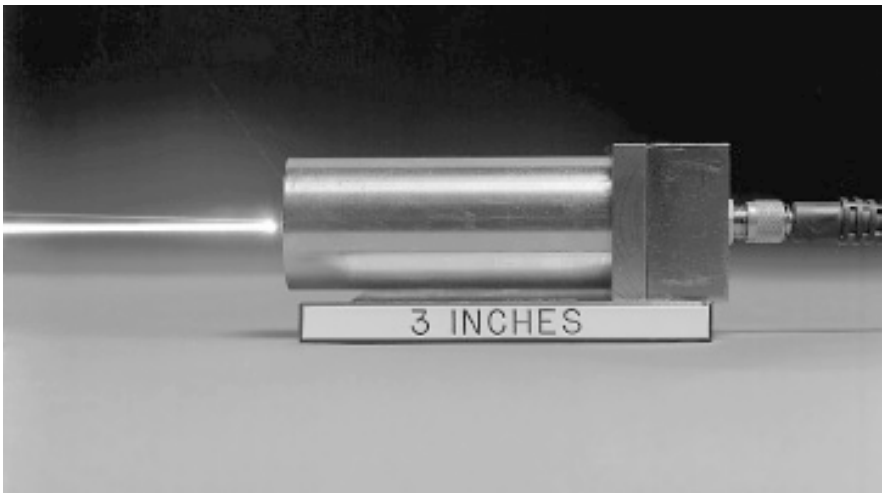

Figure 2: Packaged high power microlaser which can include up to four nonlinear crystals for frequency conversion.

It was found that, in all eleven experiments, the experimental values for the mirror reflectivity *R* and the absorber transmission *T* were very near the predicted optimum values for their corresponding small signal gain values, as demonstrated in Figure 3. The diamonds indicate the predicted optimum values based on the equations in Section 3, while the boxes indicate the experimental values.

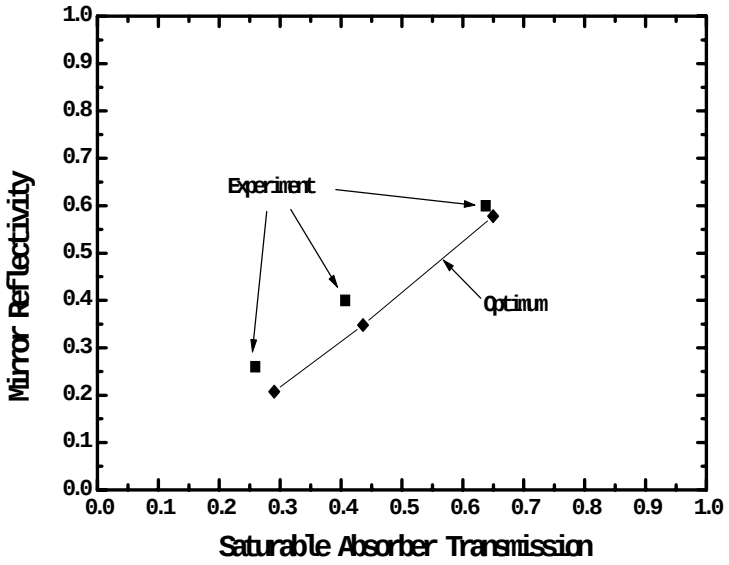

Figure 3: Comparison of experimental values (squares) of output mirror reflectivity and absorption transmission with optimum values (diamonds and line) as computed via Eqs. (6) through (9) in the text.

Figure 4 compares the experimental values for the FWHM laser pulse width (diamonds) with theoretical predictions obtained for the optimized (maximum energy) laser (solid line) and the near-optimum laser design, using the general equations in Section 2 (boxes). The agreement is generally good but degrades somewhat for the longer pulse widths.

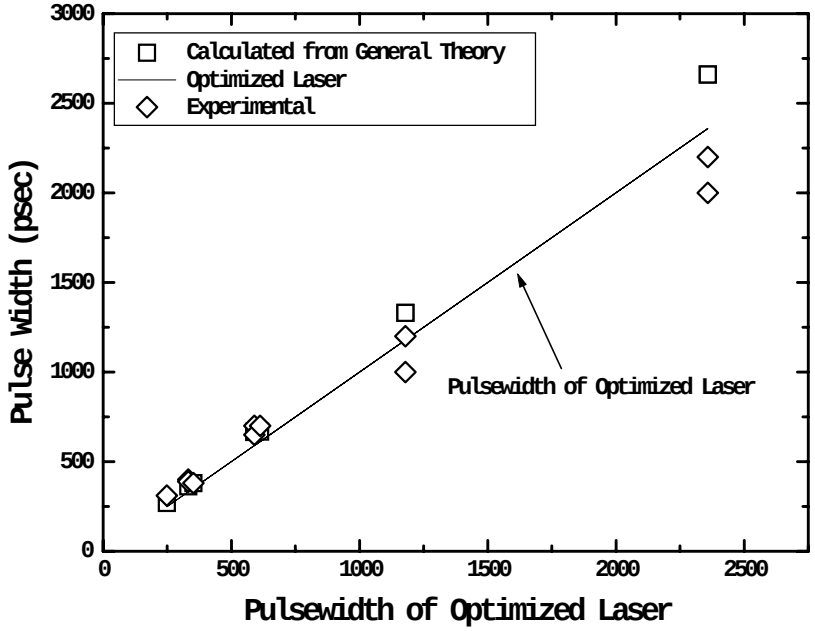

Figure 4: Comparison of theoretical pulse width predictions with actual measurements for the eleven experiments listed in Table 2. The solid line represents the computed pulse width for the energy-optimized laser as determined by the equations in Section 3. The solid diamonds represent the measured values, whereas the nearly overlapping square boxes represent the values computed using the actual mirror reflectivity and absorber transmission in the general (non-optimized) equations in Section 2. Agreement with experiment is generally good but degrades for the longer pulse widths.

Figure 5 gives a comparison of the measured energy (diamonds) vs calculated energy (squares) assuming the effective TEM_{00} mode beam area, A_{00}. The experiment number (1-11), as defined in Table 2, is plotted on the x-axis. We note that the theoretical and experimental values display the same qualitative behavior, but the measured pulse energies are substantially larger than the theoretically predicted values. Furthermore, the discrepancy cannot be eliminated by a single scale factor applied equally to all experiments, as can be seen from the semi-log plot. If one computes the total usable energy stored within this area via the equation [2]

$$E_u = \frac{h\nu A_{00} \ln G_0}{\gamma\sigma} = F_{sat} A_{00} \ln G_0 \tag{13}$$

and notes that this effective area only contains 62.3% of the energy in the gaussian pulse, one would not expect the single-pulse energy to exceed the value

$$E_{\max} = \frac{F_{sat}^{gain} A_{00} \ln G_0}{0.623}, \tag{14}$$

which is plotted as the solid line in Figure 5. Note that this curve matches the observed pulse energies fairly well for pump powers between 5 and 10 W, but still underestimates the pulse energies at the highest pump powers (experiments 10 and 11) by roughly a factor of 2. The agreement between experiment and theory is greatly improved for these last two experiments if the beam is assumed to be flattened by the saturation and largely contained within the minimum pump diameter of 125 μm, as indicated by the two circular data points in Figure 5. Thus, it would

appear that, at the higher pump powers (>5 W), the net gain in the wings of the gaussian pulse continue to feed the pulse buildup until the beam center is driven into complete saturation.

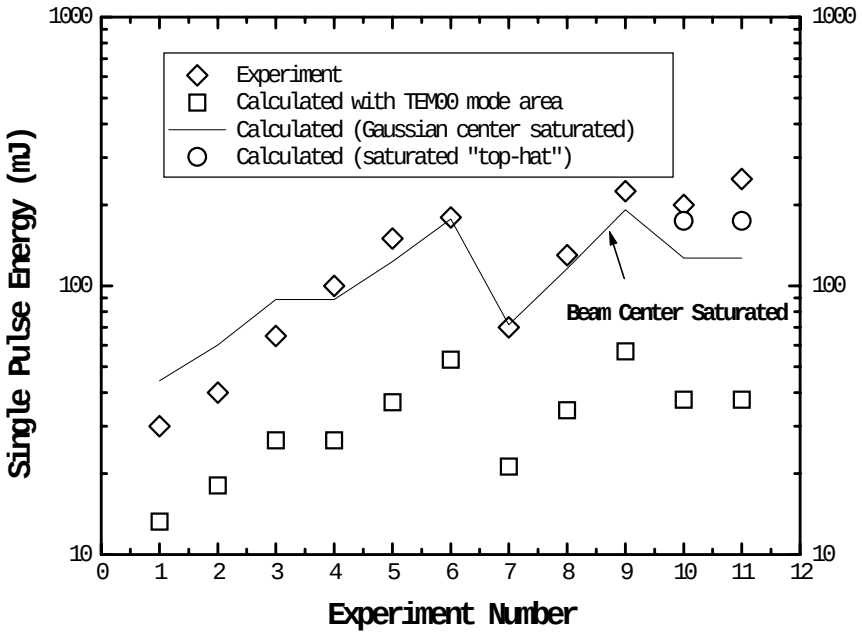

Figure 5: Measured single pulse energies (diamonds) are compared with the predicted values (boxes) where the effective TEM_{00} mode area has been substituted for the area *A* in the plane-wave model. The solid line gives the predicted upper energy limit if the residual gain in the gaussian wings drives the beam center into hard saturation. Also shown is the predicted energy for experiments 10 and 11 (circles) if one assumes that the center of the beam takes on a "flat-top", rather than gaussian, profile under conditions of complete saturation.

We can define an "effective diameter" as the diameter of a uniform beam that correctly replicates the experimentally measured energies in our plane wave model. The effective beam diameter is obtained by substituting the measured energies into equation (1) and solving for the effective beam area $A_{\text{eff}} = \pi D_{\text{eff}}^2/4$.

It is instructive to plot this effective diameter against other known dimensions such as the measured gaussian beam diameter and the minimum pump diameter. Figure 6 provides a plot of the effective beam diameter (boxes) and the measured gaussian diameter (diamonds) vs experiment number. Also indicated on the plot is the minimum pump diameter, which was typically located just inside the entrance Nd:YAG crystal face and took on values of 100 μm for experiments 1, 2, 3, and 7, and 125 μm for the other experiments.

Substituting the effective area (instead of the measured gaussian beam area) into Eq. (6) for the peak power gives good agreement between experiment (diamonds) and theory (boxes), as demonstrated in Figure 7a. Plotting the peak power versus pulse width instead of experiment number, as in Figure 7b, we note that the agreement is best for the longer pulse widths and that, at shorter widths, the calculated values are uniformly higher than the measured ones. This suggests that the effective value for the inversion reduction factor, γ, may be getting larger for the shorter pulse widths [9], whereas it was assumed in this analysis to be constant over all of the experiments. The parameter γ not only appears in the scale factors for energy and peak power but also influences the value of the saturation flux ratio, α, and therefore affects the pulse width computation through the latter's dependence on the value of ρ.

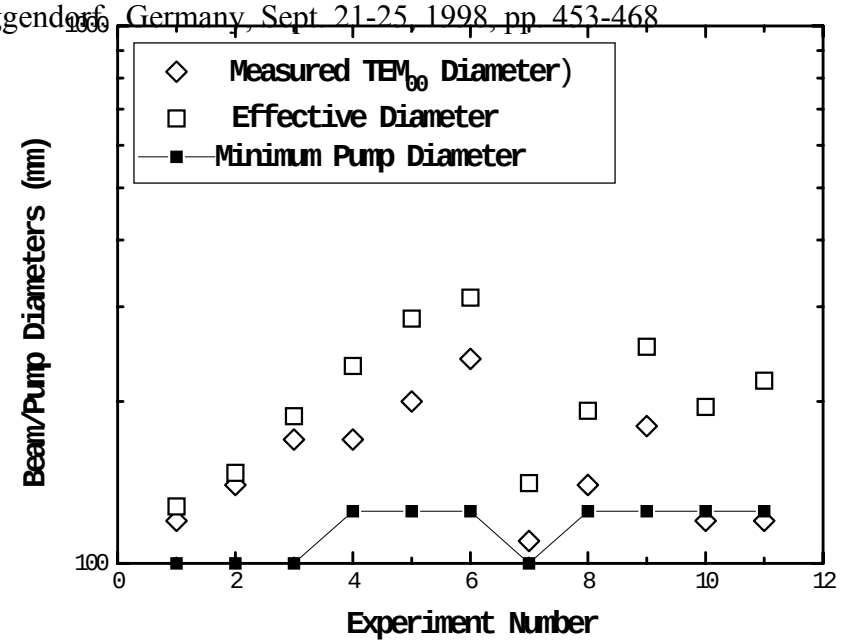

Figure 6: Effective beam diameters (boxes) and measured gaussian beam diameters (diamonds) for experiments 1 through 11. The minimum pump beam diameter in each experiment is indicated by the solid black squares connected by lines.

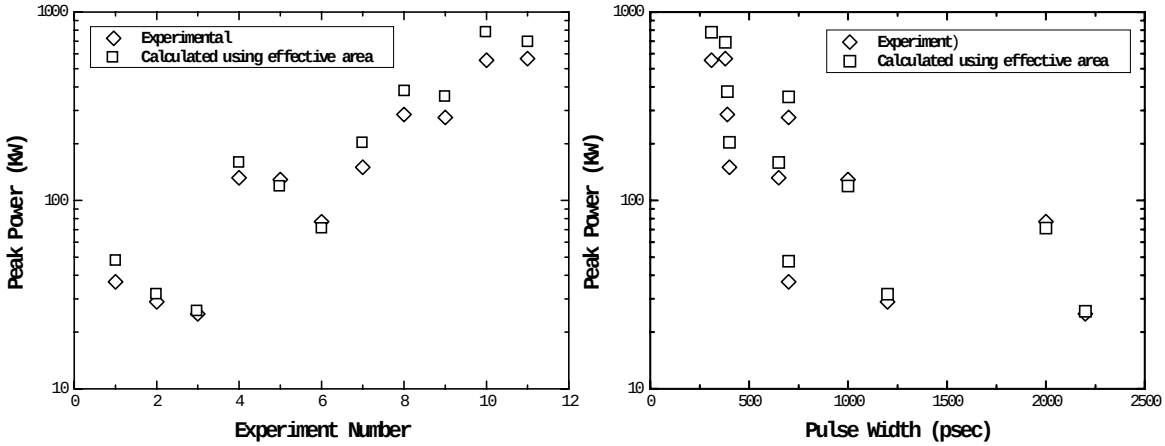

Figure 7: Comparisons of the computed (boxes) and experimental (diamonds) peak powers plotted against (a) experiment number; (b) pulse width. The effective area obtained from the energy measurements was used in the theoretical computation. Note that the best agreement is obtained for the longer pulse widths ($\geq$ 1000 psec).

6. SUMMARY

We have compared the predictions of a theoretical plane wave model of passively Q-switched lasers to actual measurements of laser parameters in medium to high power microchip lasers. The model allows for the inclusion of excited state absorption in the saturable medium, which results in an additional dissipative loss and reduces overall laser efficiency. The theory predicts the optimum values for output mirror reflectivity and unsaturated absorber transmission for a given small signal gain and internal dissipative loss, L, in a Nd:YAG laser with an internal Cr^{4+}:YAG Q-switch. The measured pulse widths generally agree well with the predicted values. Substitution of the

effective gaussian beam area into the plane wave model grossly underestimated the observed pulse energies and peak powers. Our studies suggest that, at the higher pump powers (>5 W), the gaussian wings can effectively draw energy from excited atoms outside the nominal TEM_{00} mode volume until the central region is driven into hard saturation. Application of this additional consideration resulted in a much improved agreement between theory and experiment. At still higher internal gains, some saturation flattening of the gaussian profile may be occurring.

REFERENCES

1. J. J. Degnan, "Optimal design of passively Q-switched microlaser transmitters for satellite laser ranging," Proc. 10th International Workshop on Laser Ranging, pp. 334-343, Shanghai, PRC, Nov. 11-15, 1996.

2. J. J. Degnan, "Optimization of passively Q-switched lasers," IEEE J. Quantum Electronics, vol. **31**, pp. 1890-1901,1995.

3. G. Xiao and M. Bass, "A generalized model for passively Q-switched lasers including excited state absorption in the saturable absorber," IEEE J. Quantum Electronics, vol. **33**, pp. 41-44, 1997.

4. A. Agnesi, S. Dell'Acqua, C. Morello, G. Piccino, G. C. Reali, and Z. Sun, "Diode-pumped Neodymium lasers repetitively Q-switched by Cr^{4+}:YAG solid-state saturable absorbers," IEEE J. Selected Topics in Quantum Electronics, vol. **1**, pp. 45-52, 1997.

5. X. Zhang, S. Zhao, Q. Wang, Q. Zhang, L. Sun, and S. Zhang, "Optimization of Cr^{4+}-doped saturable absorber Q-switched lasers," IEEE J. Quantum Electronics, vol. **33**, pp. 2286-2294, 1997.

6. M. Hercher, "An analysis of saturable absorbers," Applied Optics, vol. **6**, pp. 947-954, 1967.

7. J. J. Zayhowski, C. Dill III, C. Cook, and J. L. Daneu, "Mid- and high-power passively Q-switched microchip lasers," in OSA Trends in Optics and Photonics on Advanced Solid State Lasers, M. M. Fejer, U. Keller, and H. Injeyan, eds. (Optical Society of America, Washington DC, 1999), to be published.

8. J. J. Zayhowski, "Passively Q-switched microchip lasers and applications," Rev. Laser Eng., vol. **26**, pp. 841-846, 1998.

9. J. J. Degnan, D. B. Coyle, and R. B. Kay, "Effects of thermalization on Q-switched laser properties," IEEE IEEE J. Quantum Electronics, vol. **34**, pp. 887-899, 1998.

10. Z. Burshtein, P. Blau, Y. Kalisky, Y. Shimony, and M. R. Kokta, "Excited-state absorption studies of Cr^{4+} ions in several garnet host crystals," IEEE J. Quantum Electronics, vol. **34**, pp.292-299, 1998.

11. W. F. Krupke, M. D. Shinn, J. E. Marion, J. A. Caird, and S. E. Stokowski, "Spectroscopic, optical, and thermomechanical properties of neodymium and chromium doped gadolinium scandium gallium garnet," J. Optical Society of America, vol. **B3**, pp. 102-113, 1986.

.